JACS
JOURNAL OF THE AMERICAN CHEMICAL SOCIETY
Article
pubs.acs.org/JACS

Proton-Controlled Reduction of ZnO Nanocrystals: Effects of Molecular Reductants, Cations, and Thermodynamic Limitations

Carolyn N. Valdez,[†,‡] Alina M. Schimpf,[‡] Daniel R. Gamelin,[‡] and James M. Mayer*[,†]

[†]Department of Chemistry, Yale University, New Haven, Connecticut 06520-8107, United States
[‡]Department of Chemistry, University of Washington, Box 351700, Seattle, Washington 98195-1700, United States

Supporting Information

ABSTRACT: Charge carriers (electrons) were added to ZnO nanocrystals (NCs) using the molecular reductants $CoCp^*_2$ and $CrCp^*_2$ [Cp^* = η^5-pentamethylcyclopentadienyl]. The driving force for electron transfer from the reductant to the NCs was varied systematically by the addition of acid, which lowers the energy of the NC orbitals. In the presence of excess reductant, the number of electrons per NC ($\langle n_e^- \rangle$) reaches a maximum, beyond which the addition of more acid has no effect. This $\langle n_e^- \rangle_{max}$ varies with the NC radius with an r^3 dependence, so the density of electrons ($\langle N_e^- \rangle_{max}$) is constant over a range of NC sizes. $\langle N_e^- \rangle_{max} = 4.4(1.0) \times 10^{20}$ cm^{-3} for $CoCp^*_2$ and $1.3(0.5) \times 10^{20}$ cm^{-3} for the weaker reducing agent, $CrCp^*_2$. Up until the saturation point, the addition of electrons is linear with respect to protons added. This linearity contrasts with the typical description of hydrogen atom-like states (S, P, etc.) in the conduction band. The 1:1 relationship of $\langle n_e^- \rangle$ with protons per NC and the dramatic dependence of $\langle N_e^- \rangle_{max}$ on the nature of the cation (H^+ vs $MCp^*_2{}^+$) suggest that the protons intercalate into the NCs under these conditions. The differences between the reductants, the volume dependence, calculations of the Fermi level using the redox couple, and a proposed model encompassing these effects are presented. This study illustrates the strong coupling between protons and electrons in ZnO NCs and shows that proton activity is a key parameter in nanomaterial energetics.

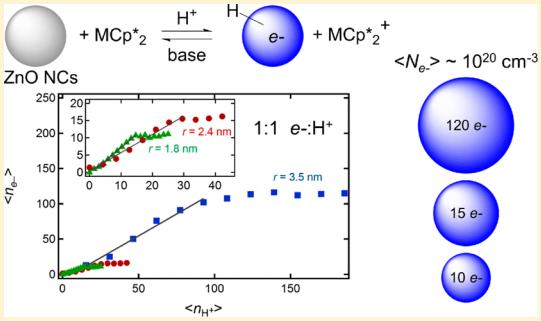

1. INTRODUCTION

The energy and density of charge carriers in semiconductor nanomaterials are critical factors in their use in electronic, optoelectronic, and plasmonic devices, energy technologies, and other applications. Extra carriers, more commonly electrons rather than holes, can be introduced into semiconductor materials by various procedures. The extra carriers affect the physical properties of the nanomaterials and are typically chemically reactive, which is critical to applications from artificial photosynthesis (solar fuels) and dye-sensitized solar cells (DSSCs) to self-cleaning coatings. For nanoscale zinc oxide (ZnO) and other oxides/chalcogenides,[1] electrons have been added by photochemistry[2−6] or electrochemistry,[7] with dihydrogen (in bulk materials),[8,9] and by aliovalent-induced,[10−17] vacancy-induced,[18−20] and remote doping.[21−27] Remote doping refers to the use of an external redox reagent, typically in solution, to add carriers. In many cases, these treatments allow fine control of the density of carriers. This chemical reactivity is particularly important on the nanoscale because the majority of the material is at or near the surface. Nanocrystals (NCs) can be treated like molecular reductants,[28] with the additional advantages that they can store multiple electrons per NC and their electronic structure can be easily tuned. Free carriers in ZnO nanocrystals have been investigated using optical, electron paramagnetic resonance (EPR), and magnetic circular dichroism spectroscopies.[2,5,6,29] The most common method of carrier generation is photoreduction, in which a photogenerated valence band hole is quenched by a chemical reductant.[2−4,22,30] Early studies of the remote doping of colloidal ZnO include those from Henglein using donors prepared radiolytically[2] and from Guyot-Sionnest using sodium biphenyl.[21]

We use aprotic solvents so that the electron/proton/NC stoichiometry can be determined and the number of added charge balancing ions (protons) can be controlled. Given the many insights gained from studying the charge carriers, the role of charge balancing ions is becoming recognized.[31,32] Charge balancing ions are necessary under steady-state conditions for many applications, but they are not often probed in many of the common methods used to study carriers, such as photoluminescence or transient absorption experiments. Achieving charge balance is likely to be of particular importance in high surface area nanomaterials with substantial concentrations of charge carriers. Protons in particular are often involved because they are ubiquitous and can originate from water or solvent, unless materials are at high temperature or vacuum. The general importance of protons has long been known, for instance, the movement of oxide band energies with pH of the contacting aqueous solution.[33,34] One report

Received: November 20, 2015
Published: January 5, 2016

DOI: 10.1021/jacs.5b12182
J. Am. Chem. Soc. 2016, 138, 1377−1385

followed the reduction of ZnO electrodes by molecular reductants in water and found that the observed rates were modulated by changes in the proton activity, using the Nernstian shift of ~60 mV/pH in the ZnO conduction band energy.[35] Hupp et al. have measured this Nernstian shift for nanoscale ZnO and TiO_2 electrodes over a remarkably wide range of proton activities.[36] Although there are many studies such as these on protons in bulk materials, a detailed, atomic-level understanding is still unavailable because proton stoichiometry is difficult to measure and control in oxide materials.

We have recently shown that protons influence the reactivity of nanoscale metal oxides, where the protons are generated in the photochemical reduction process.[37] Ethanol was used as the hole quencher, where the charges of the extra electrons in the conduction band are compensated by protons generated in the well-known oxidation of ethanol ($CH_3CH_2OH + h\nu \rightarrow CH_3CHO + 2e^- + 2H^+$). For ZnO NCs, multiple electrons per NC are accumulated[30,38,39] by this process, which we recently showed to reach a maximum that depends on the hole quencher.[6] The maximum number of electrons per NC, $\langle n_e^- \rangle_{max}$, was also found to scale with NC volume. Therefore, the maximum photochemically attainable carrier density, $\langle N_e^- \rangle_{max}$, is independent of the size of the NC.[6]

This study examines the equilibrium remote doping of ZnO nanocrystals suspended in an aprotic, low-polarity solvent (1:1 toluene/THF). The experiments reported here build on our initial qualitative report that added protons shift the effective redox potential of ZnO NCs.[23] We report quantitative analysis of the electron/proton stoichiometry, determining the energy and density of the electron charge carriers as a function of protons added. Our development of methods to retain NC solubility under these conditions has allowed studies with many acid equivalents per NC and a range of NC sizes. These advances led to the observation of a maximum electron density, related to the maximum found in photodoping experiments.[6] Since these are thermal rather than photochemical studies, they directly address the thermodynamics of the charge carriers. The constant maximum electron density and the observation that conduction band electrons are dramatically more stabilized by added protons than by large cations (from the oxidized reductant) suggest that the protons intercalate into the NCs.

2. EXPERIMENTAL SECTION

ZnO nanocrystals (NCs) were prepared as reported previously (r = 1.5 to 2 nm)[40,41] and capped with either dodecylamine (DDA) or trioctylphosphine oxide-based ligands (TOPO,[42] 90%). Larger NCs (r = 2 to 5 nm) were prepared by heating in DDA (170 °C) prior to suspension in toluene or capping with TOPO.[41] All reactions with the NCs after synthesis were done under an inert atmosphere, either in a N_2-filled glovebox or in quartz cuvettes with a Kontes Teflon valve. Using a molar absorption coefficient derived for each size of NC, the optical spectra were used to determine the number of electrons. At each size of NC, the absorption coefficient at 850 and 1200 nm was determined using the previously reported method,[37] via titration of photoreduced NCs with $[FeCp^*_2][BAr^F_4]$ [$BAr^F_4{}^-$ = $B(C_6H_3\text{-}3,5\text{-}(CF_3)_2)_4{}^-$] or 2,4,6-tri-*tert*-butyl-phenoxyl radical ($^tBu_3ArO^\bullet$) as the oxidant (see Figure S1). The oxidants were synthesized as reported previously.[37,43] All starting materials and reagents were purchased from Aldrich and used as received unless otherwise indicated. Brookhart's acid $[H(Et_2O)_2][BAr^F_4]$ was used as the proton source and was synthesized from $[Na][BAr^F_4]$ and HCl.[44] $CoCp^*_2$[45] and $CrCp^*_2$ were purchased from Aldrich and purified by filtration from pentane before use. The base, 1-*tert*-butyl-4,4,4-tris(dimethylamino)-2,2-bis-[tris(dimethylamino)-phosphoranylidenamino]-2λ^5,4λ^5-catenadi-(phosphazene) (P4-*t*-Bu-phosphazene), was purchased from Aldrich as a solution in hexanes and was dried and recrystallized from pentane before use. The solvent mixture for all experiments was kept at 50:50 v/v of toluene and THF for solubility of the reagents.

3. RESULTS

Upon addition of an excess of decamethylcobaltocene ($CoCp^*_2$; Cp* = η^5-$C_5(CH_3)_5{}^-$) to toluene/THF suspensions of ZnO NCs, optical spectra showed rapid appearance of the characteristic broad near-IR (NIR) absorption band of reduced ZnO and the presence of $CoCp^*_2{}^+$. The absorbance at 850 nm indicated an average number of electrons per NC $\langle n_e^- \rangle$ of ~2 for small NCs (as we reported previously for r < 2 nm)[23] and up to 10 for larger (r > 4 nm) NCs. Addition of aliquots of $CoCp^*_2$ showed that $\langle n_e^- \rangle$ reaches its maximum when there is at least a 5-fold excess of $CoCp^*_2$ relative to $CoCp^*_2{}^+$.[23,46]

Our initial studies of proton and electron addition to dodecylamine (DDA)-capped ZnO NCs were limited to small amounts of acid because precipitation occurred with excess acid.[23] We have now found two ways to overcome this precipitation issue. NCs capped with trioctylphosphine oxide-derived ligands (TOPO, 90%) are more stable, most likely because TOPO (90%) contains ligands that are anions (X-type) such as di-*n*-octylphosphonate,[42] which bind more strongly than neutral DDA (L-type ligand). NC solution stability with acid can also be substantially increased by using protonated DDA, dodecylammonium, as the proton source. Addition of the strong acid $[H(Et_2O)_2][BAr^F_4]$ to a THF solution of DDA immediately forms the dodecylammonium salt of the inert fluorinated anion, $[DDA\text{-}H][BAr^F_4]$, and free Et_2O (for simplicity, we will call this mixture DDA-H^+). Protonating the NCs with DDA-H^+ and excess DDA presumably increases the number of surface ligands after the proton is transferred to the NCs and helps to maintain the NC suspension. Direct measurement of the surface ligands and DDA-H^+ by ^1H NMR spectroscopy[47] was not possible because the changes are obscured by the large increase in free DDA.

Addition of acid to the suspension of ZnO NCs and excess $CoCp^*_2$ (Scheme 1) results in a large increase in the NIR

Scheme 1. Reduction of ZnO NCs with Metallocenes with the Addition of Acid as $[DDA\text{-}H][BAr^F_4]$

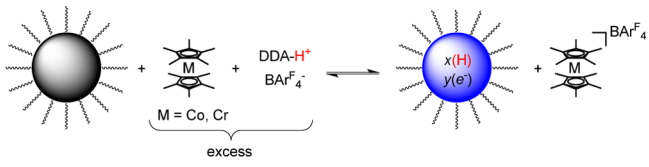

absorbance (Figure 1, top). This indicates an increase in the number of ZnO conduction band electrons due to electron transfer from the excess reductant in solution to the NCs.[23] Working at low concentrations (10^{-7} M) allows observation of a bleach of the ZnO band edge adsorption as well (see Figure S3). The changes are rapid, within the time of mixing of the reagents. This is consistent with the previous observation of rapid NC-to-NC electron transfer.[28] The resulting electron distribution between ZnO NCs and $CoCp^*_2/CoCp^*_2{}^+$ is stable, indicating an equilibrium situation controlled by thermodynamic rather than kinetic factors.

That the reduction with $CoCp^*_2$ and DDA-H^+ is an equilibrium process is further indicated by the reversibility with addition of base, as shown in Figure 1. Addition of the P4-

DOI: 10.1021/jacs.5b12182
J. Am. Chem. Soc. 2016, 138, 1377−1385

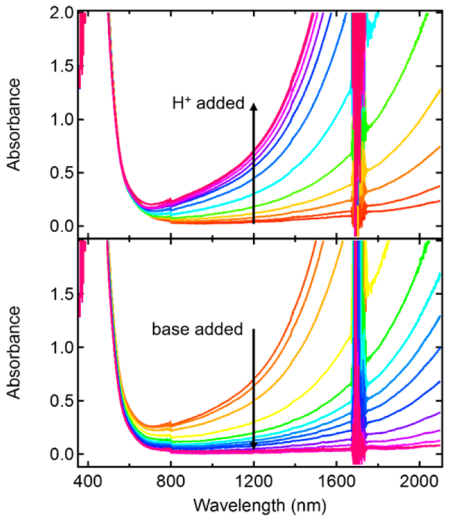

Figure 1. Reversible reduction of NCs. Top: Absorption spectra of ZnO NCs (r = 3.0 nm, 5.2 × 10^{-6} M, TOPO-capped) and $CoCp^*_2$ (6.4 × 10^{-3} M) in toluene/THF plus acid, added as a toluene/THF solution of DDA-H^+ (20 μL additions of 8.5 × 10^{-3} M, 15 equiv per NC per addition). The increase of absorbance at 510 nm and longer wavelengths is due to the tail of the NIR absorbance associated with extra electrons in ZnO NCs, the noise from 1680 to 1740 nm is from solvent absorbance, and the artifact at 800 nm is from the detector switchover. Bottom: To the sample on the top was added P_4-*t*-Bu-phosphazene base as a toluene/THF solution (20 μL additions of 8.5 × 10^{-3} M).

t-Bu-phosphazene base to a solution of NCs with excess $CoCp^*_2$ and DDA-H^+ shows a decrease in the NIR absorbance from conduction band electrons. Therefore, addition of base shifts the equilibrium such that electrons are transferred from the NCs back to $CoCp^*_2{}^+$ (Figure 1, bottom). Addition of acid or base alone (without reductant) does not introduce electrons to the NCs.

$\langle n_e^- \rangle$ with $CoCp^*_2$ is quantified using the molar absorption coefficient obtained for each size of NC. The growth of $\langle n_e^- \rangle$ is linear with respect to added protons over a wide range, reaching a maximum that is unchanged with further addition of acid (Figure 2). Over a large number of experiments and NC batches and sizes, the slopes of the linear portions are close to one electron added for each proton (between 0.5 and 1.5; Figure S5). In sum, within uncertainty, each added proton results in one electron being transferred to the ZnO NCs from the excess $CoCp^*_2$ reductant present in solution.

With a large excess of both $CoCp^*_2$ and DDA-H^+, the NCs were further reduced until a maximum was reached, $\langle n_e^- \rangle_{max}$. Additional equivalents of reductant and/or acid did not result in any increase of electrons transferred to the NCs (Figure 2). This maximum value for saturation of electrons per NC is fairly consistent for NCs of the same average size from one batch to another. However, this $\langle n_e^- \rangle_{max}$ does vary considerably with NC size (Figure 2). For example, a solution of NCs with an average radius of 1.7 nm achieves a maximum of eight electrons per NC, whereas a NC with r = 3.5 nm saturates at about 120 electrons per NC.

The $\langle n_e^- \rangle_{max}$ values can also be analyzed as added electrons per unit volume, i.e., carrier density. Here, the free carriers are electrons in the conduction band introduced via the molecular reductant. For $CoCp^*_2$ and added acid, there is a nearly constant maximum carrier density, $\langle N_e^- \rangle_{max}$, of 4.4 (±1.0) × 10^{20} cm^{-3} over NC sizes ranging from 1.5 to 5 nm in radius (Figure 3). This density is constant over more than an order of magnitude in $\langle n_e^- \rangle_{max}$ and corresponds to approximately one extra electron for every 100 Zn^{2+} ions, where the electron is delocalized over the NC. This result is very similar to our prior observations with photochemical reduction,[6] which for EtOH as the hole quencher gave $\langle N_e^- \rangle_{max}$ of 1.4(±0.4) × 10^{20} cm^{-3}. A plot of charge carriers as a function of NC radius can be fit to $\langle n_e^- \rangle_{max} = ar^p$, where p = 3 fits well, and the best fit gives p = 3.3 ± 0.4. We define maximum carrier density as $\langle N_e^- \rangle_{max}$ =

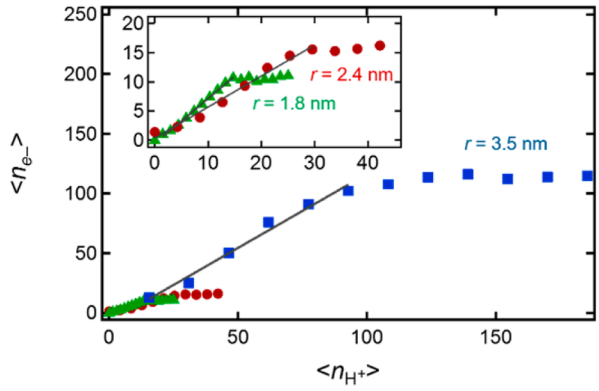

Figure 2. Dependence of NC reduction on NC size. Average number of electrons per NC ($\langle n_e^- \rangle$) versus added H^+ per NC ($\langle n_{H^+} \rangle$) for three representative NC sizes: r = 1.8 nm (green triangles), 2.4 nm (red circles), and 3.5 nm (blue squares). The corresponding slopes are about 1 e^- per added H^+ (0.8 ± 0.3, 0.7 ± 0.2, 1.4 ± 0.2, respectively). Analogous traces at different NC sizes are shown in the Supporting Information.

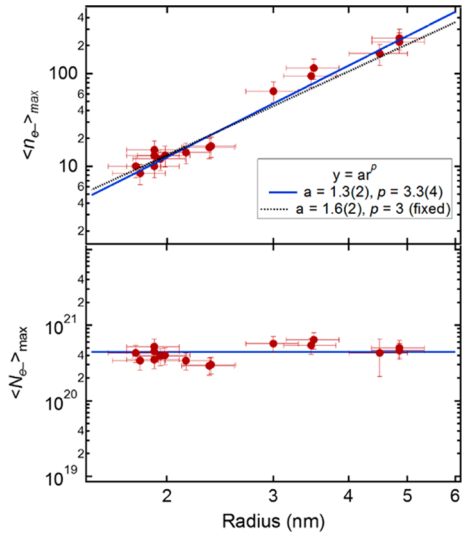

Figure 3. NC size-independent carrier density of ZnO NCs reduced with $CoCp^*_2$ and protons. Top: The maximum average number of carriers per NC, $\langle n_e^- \rangle_{max}$, attained in ZnO NCs using $CoCp^*_2$ and acid versus the NC radius. Both axes use logarithmic scales. The data are fit using the polynomial function $\langle n_e^- \rangle_{max} = ar^p$, where a phenomenological fit weighted by the error gives p = 3.3 ± 0.4 (blue line), and p = 3 (dotted black line) also fits well. NC sizes are calculated using the optical absorbance[48] (r < 3.5 nm) or from TEM (r > 3.5 nm). Uncertainties on the NC size are the standard deviation from TEM measurements or 10%, whichever was greater. Bottom: Maximum carrier density, $\langle N_e^- \rangle_{max}$, versus the NC radius. The uncertainties were estimated at 25%, and the line represents the average of all NC sizes, 4.4(1.0) × 10^{20} cm^{-3}.

DOI: 10.1021/jacs.5b12182
J. Am. Chem. Soc. 2016, 138, 1377−1385

$\langle n_e^- \rangle_{max}[(4/3)\pi r^3]^{-1}$. Then, by substitution, we can show that the maximum carrier density can be related to the fit constant a, where $\langle N_e^- \rangle_{max} = ar^3[(4/3)\pi r^3]^{-1} = 3a[4\pi]^{-1}$. The fit in Figure 3 (top) for a fixed $p = 3$ gives $a = 1.6 \pm 2$. The fit constant a is empirically derived, similar to the values of a that depend on the hole quencher (a = 0.5−2.1),[6] and in this article, a is dependent on the strength of the reductant (vide infra).

Remote doping experiments have also been performed using decamethylchromocene ($CrCp^*_2$). As reported earlier, $CrCp^*_2$ is not sufficiently reducing to donate electrons to the as-prepared ZnO NCs (−1.56 V for $CrCp^*_2$ and −1.95 V for $CoCp^*_2$ vs $Fc^{+/0}$),[49] but it does reduce the NCs upon addition of protons,[23] apparently even with one added proton (Figure S6). Using the new methods described above to prevent precipitation at high $\langle n_e^- \rangle$ and with excess acid, we have determined that $CrCp^*_2$ reduces ZnO NCs in much the same manner as that with $CoCp^*_2$. With $CrCp^*_2$, $\langle n_e^- \rangle$ again rises linearly with added acid. The slopes of the $\langle n_e^- \rangle / \langle n_{H^+} \rangle$ plots are also close to 1. Each size of NC can again be charged only to a maximum number of electrons even in the presence of excess acid and reductant. $\langle n_e^- \rangle_{max}$ with $CrCp^*_2$ shows a similar dependence on size (Figure 4, top). The maximum carrier density of 1.3(±0.5) × 10^{20} cm^{-3} is again independent of size (Figure 4, bottom). This carrier density is ca. 3 times smaller than the maximum attained with $CoCp^*_2$.

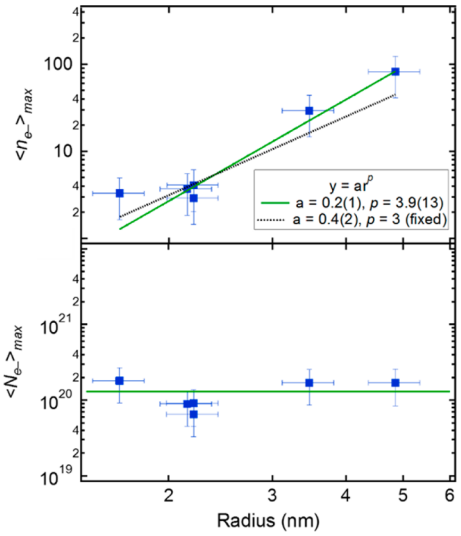

Figure 4. NC size-independent carrier density of ZnO NCs reduced with $CrCp^*_2$ and protons. Top: The maximum average number of carriers per NC, $\langle n_e^- \rangle_{max}$, attained in ZnO NCs using $CrCp^*_2$ and acid versus the NC radius. Both axes use logarithmic scales. The data are fit using the polynomial function $\langle n_e^- \rangle_{max} = ar^p$, where a phenomenological fit weighted by the error gives $p = 3.9 \pm 1.3$ (green line), and $p = 3$ (dotted black line) fits well. NC sizes are calculated using the optical absorbance[48] (r < 3.5 nm) or from TEM (r > 3.5 nm). Uncertainties on the NC size are from the standard deviation from TEM or 10%, whichever was greater. Bottom: Maximum carrier density, $\langle N_e^- \rangle_{max}$, versus the NC radius. The value of $\langle n_e^- \rangle_{max}$ was calculated from titration with excess $CrCp^*_2$ and acid, and uncertainties were estimated at 50%. The line represents the average of all NC sizes, 1.3(±0.5) × 10^{20} cm^{-3}.

4. DISCUSSION

4.1. Coupling Electron and Proton Transfers: The Importance of Charge Balance. The experiments reported here show that the addition of electrons to ZnO NCs is tightly coupled to the addition of protons under our conditions. These conditions involve the addition of acid, as $[DDA\text{-}H][BAr^F_4]$, to toluene/THF suspensions of ZnO NCs with excess reductant, MCp^*_2. In all cases, the number of electrons added to the NCs rises linearly with the number of protons added and then reaches a maximum. Deviations from linearity at low $\langle n_{H^+} \rangle$ in the larger NC samples are caused by an impurity in $CoCp^*_2$ (see Supporting Information, Figure S7). All indications are that the electron and proton transfer processes examined here are at chemical equilibrium, since the reduction occurs rapidly, the final solutions are stable, the same reduction is obtained independent of the order of addition, and the electron transfer is reversed upon addition of base. The observation of a maximum charging density is very similar to our prior observation that $\langle n_e^- \rangle_{max}$ in photodoped ZnO NCs scales with nanocrystal volume, yielding constant maximum electron densities over all nanocrystal sizes.[6] This similarity is noteworthy because the $\langle n_e^- \rangle_{max}$ values from photodoping could be determined by photostationary states and would then not reflect true thermodynamic equilibria.

The reason that electron and proton transfers are coupled is likely for charge balance. The thermochemical preference for charge balance has long been discussed in molecular proton-coupled electron transfer (PCET) processes.[50−53] As another example, charge balance has long been known to be critical to electron transfer in and out of polymer films on electrodes.[54] In the ZnO NC system discussed here, the key role of charge balance is implicated by the observation that roughly one electron is added for each proton added to the solution.

Prior to reaching $\langle n_e^- \rangle_{max}$, the linear increases in $\langle n_e^- \rangle$ with added protons (Figure 2) have slopes between 0.5 and 1.5 e^-/H^+, with an average $\langle n_e^- \rangle / \langle n_{H^+} \rangle$ slope of 0.9 ± 0.3. The deviations from one are likely due to experimental issues, including small variations in the NC suspensions from sample to sample, as some may have trace base (perhaps surface hydroxide), and variations in trace impurities in solvents and reagents at the sub-10^{-5} M level (see Supporting Information p. S7 for further discussion). The linear and roughly 1:1 e^-/H^+ behavior is perhaps surprising from an electronic structure perspective, as discussed below, but it is required if charge balance dictates the NC reactivity.

We anticipate that charge balance and PCET play key roles in many processes that involve redox reactions of nanoscale semiconductors. It could be argued that the experiments here differ from most applications in that acidic protons have intentionally been added, but protons will be present at any material/solution interface given the ubiquity of water. In addition, any added electron must have a charge balancing cation that likely plays a role in the overall energetics of e^- addition; for example, before the addition of acid, the charge balancing cation is $MCp^*_2{}^+$. The 1:1 e^-/H^+ equilibrium stoichiometry from charge balance provides a rationalization of the well-known dependence of band edge energies on the pH of contacting aqueous solutions.[33,34] As emphasized by Hupp, the 60 mV shift per pH unit is the Nernstian shift expected for a 1:1 e^-/H^+ process such as $TiO_2 + e^- + H^+ \rightarrow TiOOH$.[36,55−58] Charge balance seems likely to be increasingly important when there are many electrons per nanoparticle and high carrier densities. Charge balance drives lithium intercalation into nanoscale oxides, as in lithium batteries.[59−61] High carrier densities often occur under the steady-state conditions of many devices. In TiO_2 DSSCs, for instance, the steady-state

DOI: 10.1021/jacs.5b12182
J. Am. Chem. Soc. 2016, 138, 1377−1385

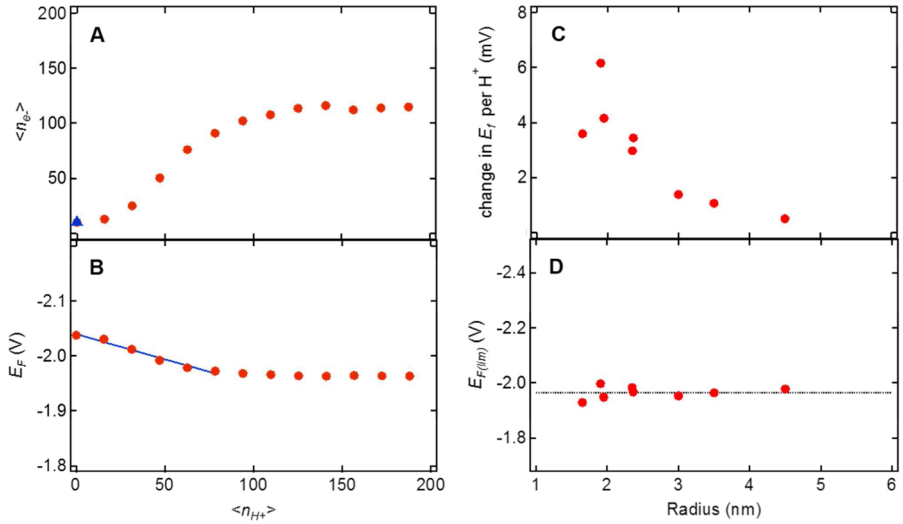

Figure 5. Estimation of NC Fermi level. (A) Plot of $\langle n_e^- \rangle$ of ZnO NCs (r = 3.5 nm) with $CoCp^*_2$ as the reductant as a function of $\langle n_{H^+} \rangle$ (H^+ per NC), where the triangle represents $\langle n_e^- \rangle$ before addition of acid (the same data as that plotted in Figure 2). (B) Fermi level of the reduction of ZnO NCs calculated with eq 1, using the same data as that plotted in panel A. The Fermi level is modified by the ratio of $CoCp^*_2$ to $CoCp^{*+}_2$; the slope of this relationship (blue line) is plotted in panel C. At the maximum carrier density, E_F saturates, represented in panel D as $E_{F(lim)}$. (C) Slope of E_F change per H^+ added plotted as a function of NC size. (D) Calculated $E_{F(lim)}$ for various NC sizes, where the dashed line shows the average $E_{F(lim)}$ as −1.97 V.

concentration of conduction band/trap state electrons is on the order of 10^{18} cm^{-3}, which corresponds to one extra electron per ~3000 titanium atoms.[62] The maximum charging density of 4.4(1.0) × 10^{20} cm^{-3} for protonated ZnO and $CoCp^*_2$ corresponds to one extra electron for every 100(20) Zn^{2+} ions (a unit cell volume of 47.66 $Å^3$ and two ZnO units per unit cell gives 4.2 × 10^{22} Zn atoms cm^{-3}).

4.2. Estimating the NC Chemical Potential. The number of electrons per NC reaches a saturation point, $\langle n_e^- \rangle_{max}$, which is independent of the amount of excess of both the reductant and the acid. $\langle n_e^- \rangle_{max}$ varies with the volume of the NCs (r^3), so the same maximum carrier density $\langle N_e^- \rangle_{max}$ is reached with a given reductant, independent of NC size. The marginal, i.e., highest energy, electron has a chemical potential equal to the Fermi energy (E_F) in these NCs.[63] At equilibrium, the chemical potential of the NCs is equal to the solution potential of the molecular redox couple. To a first approximation, the solution potential is given by the formal potential of the reductant and the ratio of MCp^{*+}_2 to MCp^*_2 in solution via the Nernst equation (eq 1).[64] This method to determine E_F independently of electron counting in the semiconductor has been adapted from that used by Kamat for TiO_2 and CdSe.[65,66] We note that this analysis is only an approximation as it depends on the absolute concentration of reductant in solution initially, but it is useful as a method to convert between stoichiometry ($\langle N_e^- \rangle_{max}$) and a chemical potential (energy) scale.

As acid is added to solutions containing NCs and $CoCp^*_2$, the $[CoCp^{*+}_2]_{eq}/[CoCp^*_2]_{eq}$ ratio increases. Thus, addition of acid causes the E_F of the system to decrease as electrons flow from the $CoCp^*_2$ to the NCs (Figure 5B). The drop in E_F reflects the less reducing conditions and stabilization of the added electrons by the positive charge of the protons.

$$E_F = -1.95 + 0.059 \log\left[\frac{MCp^{*+}_{2_{eq}}}{MCp^{*}_{2_{eq}}}\right] \quad (V \text{ vs } Fc^+/Fc) \qquad (1)$$

Plots of E_F vs $\langle n_{H^+} \rangle$ have a linear portion before saturation is reached (Figure 5B). We note that this is the same data as that in Figure 3, but it is analyzed according to eq 1. The slope of this linear portion, the change in E_F per H^+ ($\partial E_F/\partial \langle n_{H^+} \rangle$), is plotted in Figure 5C. This slope is slightly affected by the amount of MCp^*_2 initially present, but the general trend is that the change in E_F per H^+ is greater for smaller NCs than for larger NCs. In other words, the Fermi level is more sensitive to each added proton for smaller NCs. This is reasonable, as a single proton will be a greater perturbation to a small NC than a larger one.

After no additional carriers can be added to the NCs, the Fermi level reaches a limiting value ($E_{F(lim)}$; horizontal portion of Figure 5B near −2.0 V). Essentially the same $E_{F(lim)}$ is found for all sizes of NCs (Figure 5D) because roughly the same $[MCp^{*+}_2]_{eq}/[MCp^*_2]_{eq}$ ratio is obtained at maximum reduction. However, the absolute value of $E_{F(lim)}$ is approximate and changes slightly with the equivalents of MCp^*_2 used; for example, doubling the $[MCp^*_2]$ gives a difference in $E_{F(lim)}$ of about 20 mV (see the Supporting Information). Even with these small changes, the constancy of $E_{F(lim)}$ with NC radius (Figure 5D) is closely related to the constant carrier density, $\langle N_e^- \rangle_{max}$. A constant $E_{F(lim)}$ at $\langle N_e^- \rangle_{max}$ for different NC radii is also observed in photodoped ZnO NCs.[67]

The linear dependence of $\langle n_e^- \rangle$ on the number of added protons (Figures 2 and 5A) is surprising from an electronic structure perspective. Theory predicts that spherical quantum-confined NCs should have well-separated hydrogen atom-like orbitals in their "conduction band" (when the charge balancing cation is not considered).[4,68] These separations are indeed observed spectroscopically, but the relevant inter- and intra-band spectroscopic transitions involve no net change in overall charge and hence do not account for the effects of charge compensation encountered in the present redox reactions. In the spectroscopic model, after filling the *s*-type conduction band orbital with two electrons there should be a break in the linearity before the next six electrons fill *p*-type orbitals, etc. Our data show no evidence for such a discontinuity, even with

DOI: 10.1021/jacs.5b12182
J. Am. Chem. Soc. 2016, 138, 1377−1385

small numbers of electrons where this shell-filling model should be most evident. The data also indicate no noticeable difference between NCs that are quantum-confined ($r \leq \sim 4$ nm)[48] and those that behave like bulk ZnO. For quantum-confined ZnO NCs, one study estimated the separation between single-electron hydrogen-like levels in the CB to be ca. 400 meV for r = 2 nm NCs and ca. 200 meV for r = 4 NCs (much larger than kT at room temperature, 26 meV).[4] The presence of such gaps would have been evident in the experiments reported here.

The observed $\langle n_{e^-} \rangle$ versus $\langle n_{H^+} \rangle$ linearity could be due to the effects of surface trap states, inhomogeneous broadening due to NC size heterogeneity, or surface dipole effects. While the merits of these various explanations could be debated, it is not evident why any of them would lead to linearity and the roughly 1:1 stoichiometry. Thus, we favor the simple explanation that charge balance governs the NC reduction. We note again that, although the analysis using eq 1 is revealing to convert between stoichiometry and a chemical potential scale, $E_{F(lim)}$ depends on the absolute concentration of the reductant in solution (although to a small extent). Thus, Figure 5 is useful only as an approximation of $E_{F(lim)}$ and to compare the changes in E_F with each added proton.

Another benefit of using redox couples to add carriers, versus the typical method of photoreduction, is the ability to tune the applied potential by varying the reductant. Parallel experiments have been performed with $CoCp^*_2$ and $CrCp^*_2$. The difference in their measured reduction potentials in THF is 400 mV,[49] whereas the ratio of maximum carrier densities is 3. In other words, under equivalent conditions of NC, proton, and reductant concentrations, $CoCp^*_2$ transfers only ca. 3 times more electrons than $CrCp^*_2$. This is a surprisingly small value. If these were simple molecular electron transfer equilibria governed by the Gibbs free energy relationship $K_{eq} = e^{-\Delta G^\circ/RT}$ and $-\Delta G^\circ = -nF(E^\circ_{ox} - E^\circ_{red})$, then the 400 mV difference in reduction potentials (E°) in the reductants would predict the ratio of equilibrium constants ($K_{eq}^{CoCp^*2}/K_{eq}^{CrCp^*2}$) to be $10^{6.7}$. However, adding multiple e^- to a NC is not the same as adding e^- to additional molecules of a molecular reagent because the effective reduction potential of the NC is not constant. The higher reducing power of $CoCp^*_2$ does not lead to $10^{6.7}$ more e^- in the NCs; rather, it leads to the introduction of higher energy electrons. Therefore, the difference in driving force between the reactions ($\Delta\Delta G^\circ$) is not a simple predictor of the extent of reduction. At a carrier density of $4.4(1.0) \times 10^{20}$ cm^{-3}, the last electron has an E_F, an effective reduction potential, that is 400 mV higher than the marginal electron at $1.3(0.5) \times 10^{20}$ cm^{-3}. The $\Delta(\langle N_{e^-} \rangle_{max})/\Delta E^{\circ\prime}$ for the two reductants gives $\sim 8 \times 10^{20}$ carriers cm^{-3} per volt of applied potential. This analysis shows that the electrons become progressively more difficult to add to the NCs as the carrier densities increase. This is a direct measure of how the Fermi energy changes with increased carrier density in a colloidal nanocrystal system.

4.3. Surface Protonation vs Proton Intercalation. What is the behavior of the charge balancing protons in this system at the atomic level? Are they at the surface of the NCs, as hydrogen-bonded DDA-H^+ cations or surface hydroxide groups, or do they intercalate into the lattice of the NCs? While we have no direct evidence, the intercalation interpretation most simply explains the data.

For carriers in ZnO, we and others have shown that electrons are confined within the NCs. EPR spectra of photodoped ZnO NCs suggest that the added electrons occupy orbitals that are delocalized over the whole NC. This is indicated by the dependence of g^* on the NC radius and the line broadening observed with ^{67}Zn-doped NCs.[39] Proton intercalation has been suggested to occur with reduced TiO_2, ZnO, and other metal oxides.[36] It is well-known that metal oxides are porous materials for cations, a key feature of their use in lithium batteries.[69] Most notably, Hupp suggested the "deep" intercalation of protons upon electrochemical reduction of nanoparticulate TiO_2 and ZnO electrodes.[36,55−58] Intercalation explained both the observed pH dependence of conduction band energies and the electrode weight gain of oxides measured by a quartz crystal microbalance upon reduction in the presence of H^+ versus D^+.[55,56] Calculations by Van de Walle and others,[70] as well as various experimental studies,[71] indicate that hydrogen atoms ($H^+ + e^-$) are likely common n-type dopants in bulk ZnO. The calculations indicate that the intercalated protons bind strongly to a single lattice oxide, forming a hydroxide ion. Measured rates of hydrogen diffusion in bulk ZnO, if extrapolated to ambient temperatures, would predict that H^+ should move fast enough to reach its thermodynamically most favorable position on the time scale of our experiments (seconds).[72−77] We have shown here that $\langle n_{e^-} \rangle_{max}$ is limited by the volume of the NC. This volume dependence of the electrons does not provide any direct evidence for intercalation. However, there is a 1:1 relationship between electrons and protons in this system, and it is likely that the electrons and protons are both distributed within the volume of the NC.

Perhaps the strongest argument for intercalation over surface protonation is the very large difference in electron addition between H^+ and $MCp^*_2{}^+$ cations. From a continuum electrostatics point of view, the difference in size between these two cations is quite small for a r = 4.9 nm NC. Yet, $CoCp^*_2$ adds over 200 electrons to r = 4.9 nm NCs when protons balance the charge versus 40 electrons when $CoCp^*_2{}^+$ is the cation. An alternative scenario to explain the differences between the cations could invoke some sort of protonated surface trap state, different than what is present with an ion-paired surface $CoCp^*_2{}^+$. However, this is not evident from the EPR spectra. Very similar EPR spectra are seen for the conduction band electrons in Al^{3+}-doped ZnO (AZO) NCs,[15] where the charge balance is achieved by the aliovalent dopant inside the NC, not on the surface. In our view, these arguments together are strongly suggestive of proton intercalation throughout the NC upon charging.

It is remarkable that the added protons have such a strong effect on NC reduction because the NCs appear to have a significant number of surface hydroxyl groups from their hydrolytic synthesis.[41] The results reported here show that these surface protons do not substantially stabilize electrons that come from $CoCp^*_2$. One possible explanation is that the surface protons are in different sites from those populated upon addition of acid and that movement of the original surface protons away from their sites is energetically too costly. For instance, movement of the proton from surface hydroxide groups that are terminal ligands to zinc (in an atop site, Zn-OH) would be very unfavorable. Deprotonation would leave a high-energy terminal oxo ligand, which is unknown for molecular zinc compounds (in fact, for any of the transition metals in groups 9 and 10).[78,79] Studies that provide direct insight into the proton locations are needed to address this issue.

DOI: 10.1021/jacs.5b12182
J. Am. Chem. Soc. 2016, 138, 1377−1385

4.4. Working Model of the Effect of Added Protons.

The increase in $\langle n_e^- \rangle$ with added protons and the considerations above suggest a simple band interpretation (Figure 6). The electrons transferred from $CoCp^*_2$ occupy orbitals in the ensemble of NCs that behave like a band. This is based on the smooth rise in $\langle n_e^- \rangle$ with $\langle n_{H^+} \rangle$, which seems to be inconsistent with filling orbitals that are widely separated in energy. In the band picture, the key parameter is the carrier density and not the number of electrons. As acid is added, the energies of the bands decrease, creating a new equilibrium state with higher $\langle N_e^- \rangle$. This decrease in band energies with the addition of stoichiometric protons in toluene is related to the typical decrease in band energies with proton activity (pH) for oxide semiconductors in contact with aqueous solutions.[33]

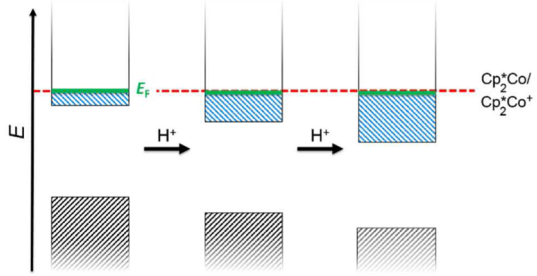

Figure 6. Schematic depiction of the effect of protons on the energetics of ZnO NCs with excess reductant. Under these conditions, the Fermi energy of the solution (E_F), indicated by the red dashed line, is roughly constant (see Section 4.3), with a slight decrease that relates to Figure 5. The hatched areas indicate energy ranges where the orbitals are occupied by electrons, with the lower black hatching being the filled valence band and the upper blue hatched area representing the added conduction band electrons. The leftmost band diagram represents an equilibrium mixture of NCs and excess $CoCp^*_2$, and the arrows indicate the equilibrium changes as acid is added.

Experiments at lower NC concentrations (necessary due to the large extinction coefficient of the band edge absorption) suggest that there is a Moss–Burstein shift of the absorption band edge, as predicted by this model (Figure S3). A similar scheme describes the change in In_2O_3 NC band positions with aliovalent Sn^{4+} doping to make n-type ITO NCs.[80]

This scheme fails to explain why an $\langle N_e^- \rangle_{max}$ is reached with excess acid. Some other feature is preventing further stabilization of the NC orbitals beyond a certain amount of protons. There could be electron–electron repulsion in the NCs that becomes proton-independent at high carrier densities. It follows that a weaker reductant will become isoergic with the electron–electron repulsion energy of the NCs at a lower potential than the more potent reductant, which is observed for $CoCp^*_2$ versus $CrCp^*_2$. Alternatively, the energetic cost of forming interstitial H^+ could become too large beyond the critical density. Since this is a PCET process, the energetics involve both protons and electrons, and the scheme depicted above does not fully explain both. Studies are underway to analyze the effects of other cations on the remote doping of ZnO NCs, which should shed additional light on this issue.

5. CONCLUSIONS

The addition of electrons from a molecular reductant to ZnO nanocrystals (NCs) is dramatically enhanced by the presence of protons. Optical monitoring and stoichiometric addition of acid allows for a determination of the amount and potential energy of the added electrons as a function of the number of protons. The number of electrons transferred to the NCs roughly equals the number of protons added to the solution, up to a maximum number of electrons per NC, $\langle n_e^- \rangle_{max}$, depending on the NC size and strength of the reductant. For a given reductant, $\langle n_e^- \rangle_{max}$ scales with r^3, meaning that NCs of all sizes are reduced to the same maximum electron density, $\langle N_e^- \rangle_{max}$. This scaling with volume and the dramatic difference between charge balance by H^+ versus $MCp^*_2{}^+$ suggest that proton intercalation into the NC is important to the stabilization of the electrons. This maximum carrier density in chemically reduced ZnO NCs is reached when the Fermi level of the NCs matches the potential of the reductant in solution, a limit that is thermodynamically controlled. Initially, we anticipated that $\langle n_e^- \rangle_{max}$ would be a stepped function of the protons added, due to the filling of an *s*-like orbital and then *p*, etc. The linearity of the addition of electrons into the conduction band with the addition of protons and the roughly 1:1 ratio of e^-/H^+ suggest that proton–electron coupling and charge balance are more important than the discrete spacing of so-called "atom-like" orbitals within the conduction band of the NC. The simple model in Figure 6 provides a reasonable rationalization of most of the results presented here, including (i) the linear increase in the number of ZnO electrons with added protons, (ii) the small difference in maximum carrier density with $CoCp^*_2$ versus $CrCp^*_2$ despite the large difference in their reducing powers, (iii) the decrease in the Fermi energy with added protons, and (iv) the maximum carrier density being the same for different size NCs.

■ ASSOCIATED CONTENT

Supporting Information

The Supporting Information is available free of charge on the ACS Publications website at DOI: 10.1021/jacs.5b12182.

Experimental details and calculations; reduction of ZnO NCs by $CoCp^*_2$; slope of E_F vs $\langle n_{H^+} \rangle$ for a range of NC sizes; maximum carrier density on a linear scale (PDF)

■ AUTHOR INFORMATION

Corresponding Author

*james.mayer@yale.edu

Notes

The authors declare no competing financial interest.

■ ACKNOWLEDGMENTS

C.N.V. acknowledges support from the Department of Energy Office of Science Graduate Fellowship Program (DOE SCGF), made possible in part by the American Recovery and Reinvestment Act of 2009, administered by ORISE-ORAU under contract no. DE-AC05-06OR23100. We also gratefully acknowledge support from the U.S. National Science Foundation (no. CHE-1151726), the Donors of the American Chemical Society Petroleum Research Fund (51178-ND3), Yale University, and the University of Washington.

■ REFERENCES

(1) Schimpf, A. M.; Knowles, K. E.; Carroll, G. M.; Gamelin, D. R. *Acc. Chem. Res.* **2015**, *48*, 1929.
(2) Haase, M.; Weller, H.; Henglein, A. *J. Phys. Chem.* **1988**, *92*, 482.
(3) Hoyer, P.; Weller, H. *Chem. Phys. Lett.* **1994**, *221*, 379.
(4) Germeau, A.; Roest, A.; Vanmaekelbergh, D.; Allan, G.; Delerue, C.; Meulenkamp, E. *Phys. Rev. Lett.* **2003**, *90*, 097401.

DOI: 10.1021/jacs.5b12182
J. Am. Chem. Soc. 2016, 138, 1377–1385

(5) Liu, W. K.; Whitaker, K. M.; Kittilstved, K. R.; Gamelin, D. R. *J. Am. Chem. Soc.* **2006**, *128*, 3910.
(6) Schimpf, A. M.; Gunthardt, C. E.; Rinehart, J. D.; Mayer, J. M.; Gamelin, D. R. *J. Am. Chem. Soc.* **2013**, *135*, 16569.
(7) Roest, A. L.; Houtepen, A. J.; Kelly, J. J.; Vanmaekelbergh, D. *Faraday Discuss.* **2004**, *125*, 55.
(8) Theys, B.; Sallet, V.; Jomard, F.; Lusson, A.; Rommeluère, J.-F.; Teukam, Z. *J. Appl. Phys.* **2002**, *91*, 3922.
(9) Strzhemechny, Y. M.; Mosbacker, H. L.; Look, D. C.; Reynolds, D. C.; Litton, C. W.; Garces, N. Y.; Giles, N. C.; Halliburton, L. E.; Niki, S.; Brillson, L. J. *Appl. Phys. Lett.* **2004**, *84*, 2545.
(10) Buonsanti, R.; Llordes, A.; Aloni, S.; Helms, B.; Milliron, D. *Nano Lett.* **2011**, *11*, 4706.
(11) De Trizio, L.; Buonsanti, R.; Schimpf, A. M.; Llordes, A.; Gamelin, D. R.; Simonutti, R.; Milliron, D. J. *Chem. Mater.* **2013**, *25*, 3383.
(12) Diroll, B. T.; Gordon, T. R.; Gaulding, E. A.; Klein, D. R.; Paik, T.; Yun, H. J.; Goodwin, E. D.; Damodhar, D.; Kagan, C. R.; Murray, C. B. *Chem. Mater.* **2014**, *26*, 4579.
(13) Kanehara, M.; Koike, H.; Yoshinaga, T.; Teranishi, T. *J. Am. Chem. Soc.* **2009**, *131*, 17736.
(14) Liang, X.; Ren, Y.; Bai, S.; Zhang, N.; Dai, X.; Wang, X.; He, H.; Jin, C.; Ye, Z.; Chen, Q.; Chen, L.; Wang, J.; Jin, Y. *Chem. Mater.* **2014**, *26*, 5169.
(15) Schimpf, A. M.; Ochsenbein, S. T.; Buonsanti, R.; Milliron, D. J.; Gamelin, D. R. *Chem. Commun.* **2012**, *48*, 9352.
(16) Wang, T.; Radovanovic, P. V. *J. Phys. Chem. C* **2011**, *115*, 406.
(17) Ye, X.; Fei, J.; Diroll, B. T.; Paik, T.; Murray, C. B. *J. Am. Chem. Soc.* **2014**, *136*, 11680.
(18) Dorfs, D.; Härtling, T.; Miszta, K.; Bigall, N. C.; Kim, M. R.; Genovese, A.; Falqui, A.; Povia, M.; Manna, L. *J. Am. Chem. Soc.* **2011**, *133*, 11175.
(19) Manthiram, K.; Alivisatos, A. *J. Am. Chem. Soc.* **2012**, *134*, 3995.
(20) Zhao, Y.; Pan, H.; Lou, Y.; Qiu, X.; Zhu, J.; Burda, C. *J. Am. Chem. Soc.* **2009**, *131*, 4253.
(21) Shim, M.; Guyot-Sionnest, P. *Nature* **2000**, *407*, 981.
(22) Shim, M.; Guyot-Sionnest, P. *J. Am. Chem. Soc.* **2001**, *123*, 11651.
(23) Valdez, C. N.; Braten, M.; Soria, A.; Gamelin, D. R.; Mayer, J. M. *J. Am. Chem. Soc.* **2013**, *135*, 8492.
(24) Palomaki, P. K. B.; Miller, E. M.; Neale, N. R. *J. Am. Chem. Soc.* **2013**, *135*, 14142.
(25) Koh, W.-k.; Koposov, A. Y.; Stewart, J. T.; Pal, B. N.; Robel, I.; Pietryga, J. M.; Klimov, V. I. *Sci. Rep.* **2013**, *3*, 2004.
(26) Jeong, K. S.; Deng, Z.; Keuleyan, S.; Liu, H.; Guyot-Sionnest, P. *J. Phys. Chem. Lett.* **2014**, *5*, 1139.
(27) Wheeler, L. M.; Neale, N. R.; Chen, T.; Kortshagen, U. R. *Nat. Commun.* **2013**, *4*, 2197.
(28) Hayoun, R.; Whitaker, K. M.; Gamelin, D. R.; Mayer, J. M. *J. Am. Chem. Soc.* **2011**, *133*, 4228.
(29) Schimpf, A. M.; Thakkar, N.; Gunthardt, C. E.; Masiello, D. J.; Gamelin, D. R. *ACS Nano* **2014**, *8*, 1065.
(30) Wood, A.; Giersig, M.; Mulvaney, P. *J. Phys. Chem. B* **2001**, *105*, 8810.
(31) Haque, S. A.; Tachibana, Y.; Willis, R. L.; Moser, J. E.; Grätzel, M.; Klug, D. R.; Durrant, J. R. *J. Phys. Chem. B* **2000**, *104*, 538.
(32) Kambe, S.; Nakade, S.; Kitamura, T.; Wada, Y.; Yanagida, S. *J. Phys. Chem. B* **2002**, *106*, 2967.
(33) Morrison, S. R. *Electrochemistry at Semiconductor and Oxidized Metal Electrodes*; Plenum Press: New York, 1980.
(34) *Semiconductor Electrodes*; Finklea, H. O., Ed.; Elsevier: New York, 1988; Vol. 55.
(35) Hamann, T. W.; Gstrein, F.; Brunschwig, B. S.; Lewis, N. S. *Chem. Phys.* **2006**, *326*, 15.
(36) Lyon, L. A.; Hupp, J. T. *J. Phys. Chem. B* **1999**, *103*, 4623.
(37) Schrauben, J. N.; Hayoun, R.; Valdez, C. N.; Braten, M.; Fridley, L.; Mayer, J. M. *Science* **2012**, *336*, 1298.
(38) Cohn, A. W.; Janßen, N.; Mayer, J. M.; Gamelin, D. R. *J. Phys. Chem. C* **2012**, *116*, 20633.
(39) Liu, W. K.; Whitaker, K. M.; Smith, A. L.; Kittilstved, K. R.; Robinson, B. H.; Gamelin, D. R. *Phys. Rev. Lett.* **2007**, *98*, 186804.
(40) Schwartz, D. A.; Norberg, N. S.; Nguyen, Q. P.; Parker, J. M.; Gamelin, D. R. *J. Am. Chem. Soc.* **2003**, *125*, 13205.
(41) Norberg, N. S.; Gamelin, D. R. *J. Phys. Chem. B* **2005**, *109*, 20810.
(42) Green, M. *J. Mater. Chem.* **2010**, *20*, 5797.
(43) Manner, V. W.; Markle, T. F.; Freudenthal, J. H.; Roth, J. P.; Mayer, J. M. *Chem. Commun.* **2008**, 256.
(44) Brookhart, M.; Grant, B.; Volpe, A. F. *Organometallics* **1992**, *11*, 3920.
(45) There is occasionally a small amount (<1%) of an impurity in $CoCp^*_2$ (max = 630 nm) that has proven to be difficult to remove, but it did not affect the values of $\langle n_{e^-} \rangle$ max (see the Supporting Information).
(46) Attempts to fit the equilibrium between ZnO NCs and $CoCp^*_2$ using a Langmuir isotherm were unsuccessful, likely because the potential of adding an additional electron increases with electron occupancy.
(47) Valdez, C. N.; Schimpf, A. M.; Gamelin, D. R.; Mayer, J. M. *ACS Nano* **2014**, *8*, 9463.
(48) Meulenkamp, E. A. *J. Phys. Chem. B* **1998**, *102*, 5566.
(49) Literature values for the $MCp^*_2{}^{+/0}$ reduction potentials in MeCN vs $Fc^{+/0}$ are − 1.46 V for $CrCp^*_2$ and − 1.91 for $CoCp^*_2$. Our measurements using cyclic voltammetry (CV) in THF, with $^nBu_4NPF_6$ supporting electrolyte, are − 1.56 V for $CrCp^*_2$ and − 1.95 V for $CoCp^*_2$ vs $Fc^{+/0}$, with roughly the same difference between them as that in MeCN.[23] Addition of toluene to the THF CV solutions caused only small changes, so the 0.39 V measured difference in potential is a good estimate of the different reducing power of these species under the 50:50 toluene/THF conditions of the remote doping experiments.
(50) Stiefel, E. I. *Proc. Natl. Acad. Sci. U. S. A.* **1973**, *70*, 988.
(51) Binstead, R. A.; Moyer, B. A.; Samuels, G. J.; Meyer, T. J. *J. Am. Chem. Soc.* **1981**, *103*, 2897.
(52) Hammes-Schiffer, S. *Chem. Rev.* **2010**, *110*, 6937.
(53) *Proton-Coupled Electron Transfer: A Carrefour for Chemical Reactivity Traditions*; Formosinho, S., Barroso, M., Eds.; Royal Society of Chemistry: Cambridge, UK, 2012.
(54) Murray, R. W. *Acc. Chem. Res.* **1980**, *13*, 135.
(55) Lemon, B. I.; Hupp, J. T. *J. Phys. Chem.* **1996**, *100*, 14578.
(56) Lemon, B. I.; Hupp, J. T. *J. Phys. Chem. B* **1997**, *101*, 2426.
(57) Yan, S. G.; Lyon, L. A.; Lemon, B. I.; Preiskorn, J. S.; Hupp, J. T. *J. Chem. Educ.* **1997**, *74*, 657.
(58) Lemon, B. I.; Lyon, L. A.; Hupp, J. T. In *Nanoparticles and Nanostructured Films: Preparation, Characterization, and Applications*; Fendler, J. H., Ed.; Wiley-VCH: New York, 1998.
(59) Kavan, L.; Kratochvilová, K.; Grätzel, M. *J. Electroanal. Chem.* **1995**, *394*, 93.
(60) Exnar, I.; Kavan, L.; Huang, S. Y.; Grätzel, M. *J. Power Sources* **1997**, *68*, 720.
(61) Aydinol, M. K.; Kohan, A. F.; Ceder, G.; Cho, K.; Joannopoulos, J. *Phys. Rev. B: Condens. Matter Mater. Phys.* **1997**, *56*, 1354.
(62) O'Regan, B. C.; Durrant, J. R. *Acc. Chem. Res.* **2009**, *42*, 1799.
(63) For a bulk material, E_F is defined as the energy at which the probability of finding an electron is 0.5. Since this definition is less valuable for molecular species and since NCs are intermediate between molecular and bulk scales, we prefer the equivalent definition in the text.
(64) Equation 1 is an approximation first because the − 1.95 V value is for THF, not for the 50:50 toluene/THF solutions used for NC measurements. Second, using the nominal concentration of $CoCp^*_2{}^+$ is an approximation because it does not take into account the tight ion pairing occurring in this low-polarity medium.
(65) Jakob, M.; Levanon, H.; Kamat, P. V. *Nano Lett.* **2003**, *3*, 353.
(66) Harris, C.; Kamat, P. V. *ACS Nano* **2010**, *4*, 7321.
(67) Carroll, G. M.; Schimpf, A. M.; Tsui, E. Y.; Gamelin, D. R. *J. Am. Chem. Soc.* **2015**, *137*, 11163.
(68) Roest, A. L.; Kelly, J. J.; Vanmaekelbergh, D.; Meulenkamp, E. A. *Phys. Rev. Lett.* **2002**, *89*, 036801.

DOI: 10.1021/jacs.5b12182
J. Am. Chem. Soc. 2016, 138, 1377−1385

(69) Goodenough, J. B.; Kim, Y. *Chem. Mater.* **2010**, *22*, 587.
(70) Van de Walle, C. G. *Phys. Rev. Lett.* **2000**, *85*, 1012.
(71) Janotti, A.; Van de Walle, C. G. *Rep. Prog. Phys.* **2009**, *72*, 126501.
(72) The diffusion of hydrogen through ZnO was extrapolated to room temperature. The resulting rate was used to calculate a time scale for diffusion across a 5 nm NC, which was on the order of seconds or milliseconds, depending on the *D* used. See refs 73−75.
(73) Thomas, D. G.; Lander, J. J. *J. Chem. Phys.* **1956**, *25*, 1136.
(74) Ip, K.; Overberg, M. E.; Heo, Y. W.; Norton, D. P.; Pearton, S. J.; Stutz, C. E.; Luo, B.; Ren, F.; Look, D. C.; Zavada, J. M. *Appl. Phys. Lett.* **2003**, *82*, 385.
(75) Nickel, N. H. *Phys. Rev. B: Condens. Matter Mater. Phys.* **2006**, *73*, 195204.
(76) This estimate likely overestimates the time required for proton movement because cation diffusion in nanostructures is typically much faster than that in bulk. See ref 77.
(77) Son, D. H.; Hughes, S. M.; Yin, Y.; Alivisatos, A. P. *Science* **2004**, *306*, 1009.
(78) Mayer, J. M. *Comments Inorg. Chem.* **1988**, *8*, 125.
(79) Winkler, J.; Gray, H. In *Molecular Electronic Structures of Transition Metal Complexes I*; Mingos, D. M. P., Day, P., Dahl, J. P., Eds.; Springer: Berlin, 2012; Vol. *142*, p 17.
(80) Schimpf, A. M.; Runnerstrom, E. L.; Lounis, S. D.; Milliron, D. J.; Gamelin, D. R. *J. Am. Chem. Soc.* **2015**, *137*, 518.

DOI: 10.1021/jacs.5b12182
J. Am. Chem. Soc. 2016, 138, 1377−1385